communications physics

Article

A Nature Portfolio journal

https://doi.org/10.1038/s42005-026-02624-5

A general model for frictional contacts in colloidal systems

Kay Hofmann [1], Kay-Robert Dormann [2], Benno Liebchen [2] & Friederike Schmid [1]

In simulations of colloidal matter, frictional contacts between particles are often neglected. For spherical colloids, such an approximation can be problematic, since frictional contacts couple translational and rotational degrees of freedom, which may affect the collective behavior of, e.g., colloids under shear and chiral active matter. Deterministic models for frictional contacts have been proposed in the granular matter community. On the colloidal scale, however, thermal fluctuations are important and should be included in a thermodynamically consistent manner. Here, we derive the correct fluctuation-dissipation relation for linear and nonlinear instantaneous frictional contact interactions. Among other, this introduces a generalized class of dissipative particle dynamics (DPD) thermostats with rotation-translation coupling. We demonstrate effects of frictional contact interactions using the examples of Poiseuille flow and motility induced phase separation in active Langevin particles.

Friction has been studied for centuries. Early important observations of frictional forces acting on macroscopic bodies on surfaces have been made by da Vinci and Amontons[1]. In the 18th century, Coulomb discovered his famous friction law[2]. Later, the role of frictional contacts between particles in many particle systems has also been intensively explored in granular matter. Here, friction induces a significant coupling between translational and rotational degrees of freedom of the particles. Commonly employed standard models describing frictional contacts in granular matter have been discussed in refs. 3–8. Characteristically, these models do not account for thermal fluctuations, which are negligibly weak for granular particles. A first model to describe dry friction in Brownian particles has been developed by de Gennes in 2005[9]. This paper also proposes an experimental realization based on granular particles in randomly vibrating plates. Such situations, which involve both frictional contacts and imposed Brownian motion, have subsequently been studied both theoretically and experimentally[10–13] and very recently also in (granular) active particles[14].

At the colloidal scale, frictional contacts have long been neglected. However, within the past decade, there has been increasing evidence that frictional contacts can play an important role in colloidal systems, in particular when they are sheared, leading to large relative velocities of adjacent colloids. In particular, the role of frictional contacts for discontinuous shear thickening in colloidal (and larger) particles has been prominently discussed. While discontinuous shear-thickening has originally been attributed to lubrication flows[15], later theoretical[16–18] and experimental[19–23] works provide evidence, that (nanoscale) repulsive and frictional forces play a key role for discontinuous shear-thickening. A popular idea is that at low pressure, the solvent in the gaps between adjacent particles keeps them apart, whereas at higher pressure, the particles overcome repulsive forces and frictional contacts become important, ultimately resulting in shear thickening. While the overall mechanism for the emergence of discontinuous shear thickening is probably comparatively involved[24], there is now strong evidence that frictional contacts play a central role for sheared colloids undergoing discontinuous shear-thickening.

Recently, frictional contacts have also been intensively studied in (colloidal) active matter systems. Similarly as in sheared systems, also in active systems the relative velocity between adjacent particles can be rather high, suggesting that frictional contacts could play an important role in these systems[25]. To describe frictional contacts, Nie et al.[25] have employed a model from the granular community, whereas Abaurrea-Velasco et al.[26,27] have developed a new model describing overdamped active particles with frictional contacts. Besides self-propelled active particles, also active spinners with frictional contacts have been studied[28].

Importantly, unlike for granular matter, for colloidal matter thermal fluctuations are important. Despite this, most models that have been used to describe frictional contacts in colloidal matter have borrowed models to describe friction from the granular community[3,6], or have developed new ones[26,27] which have been combined with standard translational and rotational additive white noise terms, similarly as for particles without frictional contacts. This may be sufficient to describe common experiments, but from a fundamental perspective, this approach leads to thermodynamically inconsistent models that may violate Onsager relations and do not obey the fluctuation dissipation theorem in the equilibrium limit. This happens for

[1]Institute of Physics, Johannes Gutenberg-Universität Mainz, Mainz, Germany. [2]Institute for Condensed Matter Physics, Department of Physics, Technische Universität Darmstadt, Darmstadt, Germany. e-mail: friederike.schmid@uni-mainz.de

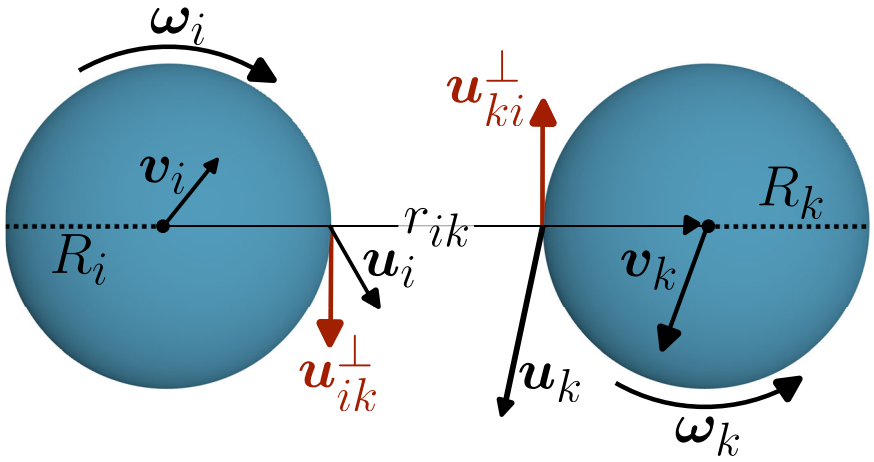

Fig. 1 | Relative tangential motion at particle contacts. Sketch of a two-particle configuration subject to tangential friction. The quantities $R_{i,j}$ and $\boldsymbol{\omega}_{i,j}$ denote the radii and angular velocities, respectively, of particles i, j. The vectors $\boldsymbol{v}_{i,j}$, $\boldsymbol{u}_{i,j}$, $\boldsymbol{u}_{i,j}^{\perp}$ represent their velocities, relative velocities, and tangentially projected relative velocities (see text).

models that account only for fluctuations that appear as a counterpart to Stokes drag, but not for the additional fluctuations that necessarily arise as a counterpart to tangential friction (frictional contacts) in colloids that are subject to a thermal bath. As we show in the present work, thermodynamic inconsistencies due to the consideration of incomplete thermal fluctuations can (wrongly) lead to the prediction of different equilibrium temperature values for the rotational and translational degrees of freedom, which both differ from the bath temperature, and are accompanied by non-Maxwell-Boltzmann velocity distributions. In nonequilibrium, for active systems, thermodynamically inconsistent treatments of frictional contacts can have severe consequences for the predicted collective behavior.

The central aim of the present work is therefore to develop a thermodynamically consistent model to describe colloidal matter with frictional contacts (active and passive). To achieve this, we develop a model that is closely related to a popular model from the granular community[5] and systematically calculate the required *multiplicative* noise term. Using particle-based simulations, we confirm that the resulting translational and angular velocity distributions are fully consistent with the predictions from statistical mechanics and both lead to temperatures that coincide with the bath temperature. To study the role of thermodynamic (in)consistencies, we explore two examples for sheared colloids and for active colloids undergoing motility-induced phase separation.

Our results could serve as a useful ingredient to model sheared colloidal suspensions, to help understand discontinuous shear thickening and to model systems of self-propelled particles as well as active[29,30] (and passive[31]) spinners with frictional contacts. The latter should be of particular interest in the context of the enormous present interest in odd hydrodynamics[32,33].

Results

Theory: modeling tangential friction interactions

Statement of the problem. We consider systems of spherical colloidal particles that interact with each other via conservative forces and surface friction forces. In addition, the particles may interact with a background medium and/or experience further driving or active forces. Specific examples will be discussed below in the subsection "Application examples". Here, we focus on the modeling of the surface friction forces.

The friction forces depend on the relative tangential velocities of the particles at the point of contact, but not necessarily in a linear manner. If two particles collide, this induces changes of both their momenta and angular momenta. As mentioned in the introduction, deterministic models for such contact forces have been discussed for centuries. On colloidal scales, however, an additional aspect comes in: Thermal fluctuations become important. Friction forces are invariably associated with random, stochastic forces, which can not be ignored on small scales, but must be included in a thermodynamically consistent manner. To ensure that passive systems without nonequilibrium driving forces reach thermal equilibrium, the frictional and the corresponding stochastic forces must satisfy a fluctuation-dissipation relation. In other words: the frictional and stochastic forces must be coupled such that, together, they act as a thermostat for the system, independent of other thermostats that may describe, e.g., the coupling to a background medium.

Our aim is to derive a general structure of thermostats that arise from tangential friction forces between particles. We will focus on Markovian forces without memory. In the granular matter literature, non-Markovian friction models have also been proposed to mimic transitions between static and dynamic friction[4,5]. Such models will not be considered here.

Structure of deterministic friction force. The general form of deterministic Markovian tangential friction forces between two spherical particles i and k with radii $R_{i,k}$, center positions $\boldsymbol{r}_{i,k}$, angular velocities $\boldsymbol{\omega}_{i,k}$, and translational velocities $\boldsymbol{v}_{i,k}$, can be constructed as follows[4]. If the particles are in contact, their surface velocities at the contact point are given by

$$\boldsymbol{u}_i = \boldsymbol{v}_i + \boldsymbol{\omega}_i \times \widehat{\boldsymbol{r}}_{ik} R_i \tag{1}$$

$$\boldsymbol{u}_k = \boldsymbol{v}_k - \boldsymbol{\omega}_k \times \widehat{\boldsymbol{r}}_{ik} R_k, \tag{2}$$

where we have defined $\widehat{\boldsymbol{r}}_{ik} = \boldsymbol{r}_{ik}/r_{ik}$ with $\boldsymbol{r}_{ik} = \boldsymbol{r}_k - \boldsymbol{r}_i$ and $r_{ik} = |\boldsymbol{r}_{ik}|$. From these expressions, we can calculate the relative tangential velocity $\boldsymbol{u}_{ik}^{\perp}$ at the contact point as the projection of the surface velocity difference, $\boldsymbol{u}_k - \boldsymbol{u}_i$, onto the tangent plane at contact (see Fig. 1), i.e., $\boldsymbol{u}_{ik}^{\perp} = \boldsymbol{P}(\widehat{\boldsymbol{r}}_{ik})(\boldsymbol{u}_k - \boldsymbol{u}_i)$ with the projection operator

$$\boldsymbol{P}(\widehat{\boldsymbol{r}}_{ik}) = \boldsymbol{1} - \widehat{\boldsymbol{r}}_{ik}\widehat{\boldsymbol{r}}_{ik}, \tag{3}$$

giving

$$\boldsymbol{u}_{ik}^{\perp} = \boldsymbol{P}(\widehat{\boldsymbol{r}}_{ik})(\boldsymbol{v}_k - \boldsymbol{v}_i) - (\boldsymbol{\omega}_i R_i + \boldsymbol{\omega}_k R_k) \times \widehat{\boldsymbol{r}}_{ik}. \tag{4}$$

Assuming that the tangential friction force at the contact point points in the direction of $\boldsymbol{u}_{ik}^{\perp}$, we model it very generally as

$$\boldsymbol{F}_i^{\mathrm{f,contact}} = -\boldsymbol{F}_k^{\mathrm{f,contact}} = f(u_{ik}^{\perp}, r_{ik})\, \widehat{\boldsymbol{u}}_{ik}^{\perp} \tag{5}$$

with $\widehat{\boldsymbol{u}}_{ik}^{\perp} = \boldsymbol{u}_{ik}^{\perp}/u_{ik}^{\perp}$, where $f(u_{ik}^{\perp}, r_{ik})$ is an arbitrary function of the relative tangential velocity and the distance between the particles. The surface force $\boldsymbol{F}_i^{\mathrm{f,contact}}$ generates a center-of-mass force and torque acting on particle i,

$$\boldsymbol{F}_{ik}^{\mathrm{f}} = \boldsymbol{F}_i^{\mathrm{f,contact}}, \ \boldsymbol{\tau}_{ik}^{\mathrm{f}} = R_i \widehat{\boldsymbol{r}}_{ik} \times \boldsymbol{F}_i^{\mathrm{f,contact}}, \tag{6}$$

which is a pair friction force and torque resulting from the friction with the particle k and can be rewritten as

$$\boldsymbol{F}^{\mathrm{f}}_{ik} = \frac{f(u^{\perp}_{ik}, r_{ik})}{u^{\perp}_{ik}} \left[\boldsymbol{P}(\widehat{\boldsymbol{r}}_{ik})(\boldsymbol{v}_k - \boldsymbol{v}_i) + \widehat{\boldsymbol{r}}_{ik} \times (\boldsymbol{\omega}_i R_i + \boldsymbol{\omega}_k R_k)\right], \tag{7}$$

$$\frac{\boldsymbol{\tau}^{\mathrm{f}}_{ik}}{R_i} = \frac{f(u^{\perp}_{ik}, r_{ik})}{u^{\perp}_{ik}} \left[\widehat{\boldsymbol{r}}_{ik} \times (\boldsymbol{v}_k - \boldsymbol{v}_i) - \boldsymbol{P}(\widehat{\boldsymbol{r}}_{ik})(\boldsymbol{\omega}_i R_i + \boldsymbol{\omega}_k R_k)\right]. \tag{8}$$

We note that the torques transmitted to the two particles i and k point in the same direction (and are in fact identical for $R_i = R_k$), whereas the forces are opposed to each other. One can easily see that the deterministic friction force always reduces the kinetic energy of the two particles during a collision, since

$$\begin{aligned} \frac{\mathrm{d}}{\mathrm{d}t} E_{\mathrm{kin}}\Big|_{\mathrm{f}} &= \frac{\mathrm{d}}{\mathrm{d}t}\frac{1}{2}\left(m_i \boldsymbol{v}_i^2 + m_k \boldsymbol{v}_k^2 + \boldsymbol{\omega}_i \boldsymbol{I}_i \boldsymbol{\omega}_i + \boldsymbol{\omega}_k \boldsymbol{I}_k \boldsymbol{\omega}_k\right)\Big|_{\mathrm{f}} \\ &= \boldsymbol{F}^{\mathrm{f}}_{ik} \cdot (\boldsymbol{v}_i - \boldsymbol{v}_k) + \boldsymbol{\tau}^{\mathrm{f}}_{ik} \cdot \boldsymbol{\omega}_i + \boldsymbol{\tau}^{\mathrm{f}}_{ki} \cdot \boldsymbol{\omega}_k \\ &= -f(u^{\perp}_{ik}, r_{ik})\, u^{\perp}_{ik} \le 0, \end{aligned} \tag{9}$$

where $m_{i,k}$ are the masses, $\boldsymbol{I}_{i,k}$ the moments of inertia of the two particles, and the subscript f refers to the fact that only the effect of friction forces is considered. No energy is dissipated in this model if $\boldsymbol{u}^{\perp}_{ik} = 0$, which corresponds to a rolling contact. Furthermore, the possibility of spinning friction is also neglected.

In addition to our analytical derivation, we have numerically verified that energy is dissipated during particle collisions (Supplementary Note 1 with Fig. S1).

Structure of corresponding stochastic force. Our goal is to construct stochastic forces such that, together with the deterministic friction forces, the configurations are Boltzmann distributed at equilibrium. To this end, we examine the corresponding Fokker-Planck equation[34].

The system of interest consists of N particles with positions $\boldsymbol{r}_i$, orientations characterized by two orthogonal unit vectors $(\boldsymbol{e}^{(1)}_i, \boldsymbol{e}^{(2)}_i)$, momenta $\boldsymbol{p}_i = m_i \boldsymbol{v}_i$, and intrinsic angular momenta $\boldsymbol{j}_i = \boldsymbol{I}_i \boldsymbol{\omega}_i$, which obey the equations of motion $\dot{\boldsymbol{p}}_i = \boldsymbol{F}_i$, $\dot{\boldsymbol{j}}_i = \boldsymbol{\tau}_i$, $\dot{\boldsymbol{r}}_i = \boldsymbol{p}_i/m_i$, and $\dot{\boldsymbol{e}}^{(\alpha)}_i = (\boldsymbol{I}_i^{-1}\boldsymbol{j}_i) \times \boldsymbol{e}^{(\alpha)}_i$. Here, $\boldsymbol{F}_i$ and $\boldsymbol{\tau}_i$ denote the total forces and torques acting on particle i. The time evolution of the N-particle distribution function $\mathcal{P}(\Gamma, t)$ with $\Gamma = \{\boldsymbol{r}_i, \boldsymbol{p}_i, \boldsymbol{e}^{(1,2)}_i, \boldsymbol{j}_i\}$ is described by a Fokker-Planck equation $\partial_t \mathcal{P} = L_{\mathrm{FP}} \mathcal{P}$. We focus on the contributions of the deterministic tangential friction force due to a frictional contact with particle k, L^{f}_{ik}, and the corresponding stochastic force, L^{R}_{ik}, to the Fokker-Planck operator L_{FP}:

$$L_{\mathrm{FP}} = \sum_{i<k} (L^{\mathrm{f}}_{ik} + L^{\mathrm{R}}_{ik}) + \text{ other contributions}, \tag{10}$$

where the sum $\sum_{i<k}$ runs over all pairs (i, k) of particles with $i < k$. The deterministic term accounts for the effect of the friction force and torque, Eqs. (7) and (8), and can be decomposed into

$$L^{\mathrm{f}}_{ik} = (\partial_{\boldsymbol{p}_k} - \partial_{\boldsymbol{p}_i})\, \boldsymbol{J}^{\mathrm{f}}_{ik,\boldsymbol{p}} - (\partial_{\boldsymbol{j}_i} R_i + \partial_{\boldsymbol{j}_k} R_k)\, \boldsymbol{J}^{\mathrm{f}}_{ik,\boldsymbol{j}} \tag{11}$$

with probability current operators

$$\begin{aligned} \boldsymbol{J}^{\mathrm{f}}_{ik,\boldsymbol{p}} =& \frac{f(u^{\perp}_{ik}, r_{ik})}{u^{\perp}_{ik}} \left(\boldsymbol{P}(\widehat{\boldsymbol{r}}_{ik}) \left(\frac{\boldsymbol{p}_k}{m_k} - \frac{\boldsymbol{p}_i}{m_i}\right)\right. \\ &\left. + \widehat{\boldsymbol{r}}_{ik} \times \left(\boldsymbol{I}_i^{-1}\boldsymbol{j}_i R_i + \boldsymbol{I}_k^{-1}\boldsymbol{j}_k R_k\right)\right), \end{aligned} \tag{12}$$

$$\begin{aligned} \boldsymbol{J}^{\mathrm{f}}_{ik,\boldsymbol{j}} =& \frac{f(u^{\perp}_{ik}, r_{ik})}{u^{\perp}_{ik}} \left(\widehat{\boldsymbol{r}}_{ik} \times \left(\frac{\boldsymbol{p}_k}{m_k} - \frac{\boldsymbol{p}_i}{m_i}\right)\right. \\ &\left. - \boldsymbol{P}(\widehat{\boldsymbol{r}}_{ik})(\boldsymbol{I}_i^{-1}\boldsymbol{j}_i R_i + \boldsymbol{I}_k^{-1}\boldsymbol{j}_k R_k)\right). \end{aligned} \tag{13}$$

We assume that it is possible to construct stochastic forces and torques $\boldsymbol{F}^{\mathrm{R}}_{ik}$ and $\boldsymbol{\tau}^{\mathrm{R}}_{ik}$ such that the corresponding Fokker-Planck operator can be decomposed in the same manner,

$$L^{\mathrm{R}}_{ik} = (\partial_{\boldsymbol{p}_k} - \partial_{\boldsymbol{p}_i})\, \boldsymbol{J}^{\mathrm{R}}_{ik,\boldsymbol{p}} - (\partial_{\boldsymbol{j}_i} R_i + \partial_{\boldsymbol{j}_k} R_k)\, \boldsymbol{J}^{\mathrm{R}}_{ik,\boldsymbol{j}} \tag{14}$$

such that

$$\left(\boldsymbol{J}^{\mathrm{f}}_{ik,\boldsymbol{p}} + \boldsymbol{J}^{\mathrm{R}}_{ik,\boldsymbol{p}}\right) \mathcal{P}_{\mathrm{B}} = 0 \tag{15}$$

$$\left(\boldsymbol{J}^{\mathrm{f}}_{ik,\boldsymbol{j}} + \boldsymbol{J}^{\mathrm{R}}_{ik,\boldsymbol{j}}\right) \mathcal{P}_{\mathrm{B}} = 0. \tag{16}$$

for the Boltzmann distribution

$$\mathcal{P}_{\mathrm{B}}(\Gamma) \propto \exp\left[-\frac{1}{k_{\mathrm{B}}T}\left(U(\{\boldsymbol{r}_i\}) + \sum_i \left(\frac{\boldsymbol{p}_i^2}{2m_i} + \frac{1}{2}\boldsymbol{j}_i \boldsymbol{I}_i^{-1} \boldsymbol{j}_i\right)\right)\right]. \tag{17}$$

In other words, we request that the Boltzmann distribution is not only the stationary solution of the equilibrium Fokker-Planck equation, but also, that all probability currents $\boldsymbol{J}^{\mathrm{R}}_{ik,\boldsymbol{p}}\, \mathcal{P}_{\mathrm{B}}$ and $\boldsymbol{J}^{\mathrm{R}}_{ik,\boldsymbol{j}}\, \mathcal{P}_{\mathrm{B}}$ vanish individually.

In general, the stochastic forces and torques will depend on the instantaneous momenta and angular momenta of particles and generate multiplicative noise. Hence, the structure of the probability currents depends on the choice of stochastic calculus[35]. Here, we will discuss three popular choices: (i) the Itô calculus, which is commonly implemented in numerical simulations, (ii) the Stratonovich calculus, which is commonly used in physical theories because it preserves the chain rule, (iii) the Hänggi-Klimontovich calculus[36–38]. Loosely speaking, they differ in their definitions how to evaluate the integrand in discrete implementations of time integrals, $\int f(t)\,\mathrm{d}t = \sum_i \left((1-\theta) f_i + \theta f_{i+1}\right)\left(t_{i+1} - t_i\right)$. The Itô calculus specifies $\theta = 0$, the Stratonovich calculus $\theta = 1/2$, and the Hänggi-Klimontovich calculus $\theta = 1$. We can account for all three possibilities by making the following Ansatz for the probability currents (see Section "Methods", Subsection "Theory"):

$$\begin{aligned} \boldsymbol{J}^{\mathrm{R}}_{ik,\boldsymbol{p}} =& k_{\mathrm{B}} T\, D(u^{\perp}_{ik}, r_{ik})^{\theta} \left(\boldsymbol{P}(\widehat{\boldsymbol{r}}_{ik}) \left(\partial_{\boldsymbol{p}_k} - \partial_{\boldsymbol{p}_i}\right)\right. \\ &\left. + \widehat{\boldsymbol{r}}_{ik} \times \left(\partial_{\boldsymbol{j}_i} R_i + \partial_{\boldsymbol{j}_k} R_k\right)\right) D(u^{\perp}_{ik}, r_{ik})^{1-\theta}, \end{aligned} \tag{18}$$

$$\begin{aligned} \boldsymbol{J}^{\mathrm{R}}_{ik,\boldsymbol{j}} =& k_{\mathrm{B}} T\, D(u^{\perp}_{ik}, r_{ik})^{\theta} \left(\widehat{\boldsymbol{r}}_{ik} \times \left(\partial_{\boldsymbol{p}_k} - \partial_{\boldsymbol{p}_i}\right)\right. \\ &\left. - \boldsymbol{P}(\widehat{\boldsymbol{r}}_{ik})(\partial_{\boldsymbol{j}_i} R_i + \partial_{\boldsymbol{j}_k} R_k)\right) D(u^{\perp}_{ik}, r_{ik})^{1-\theta}. \end{aligned} \tag{19}$$

Using the general identities $\boldsymbol{P}(\widehat{\boldsymbol{r}})^2 \boldsymbol{u} = \boldsymbol{P}(\widehat{\boldsymbol{r}})\boldsymbol{u} = -\widehat{\boldsymbol{r}} \times (\widehat{\boldsymbol{r}} \times \boldsymbol{u})$, and $\widehat{\boldsymbol{r}} \times \boldsymbol{P}(\widehat{\boldsymbol{r}})\boldsymbol{u} = \boldsymbol{P}(\widehat{\boldsymbol{r}})(\widehat{\boldsymbol{r}} \times \boldsymbol{u}) = \widehat{\boldsymbol{r}} \times \boldsymbol{u}$, which are valid for all vectors $\boldsymbol{u}$, one can easily check that Eqs. (15) and (16) are fulfilled with this choice, if the function $D(u, r)$ obeys the differential equation

$$v\, k_{\mathrm{B}} T\, \partial_u D(u, r) - D(u, r)\, u = -f(u, r) \tag{20}$$

with

$$v = (1 - \theta)\left[\left(\frac{1}{m_i} + \frac{1}{m_k}\right) + \left(\frac{R_i^2}{I_i} + \frac{R_k^2}{I_k}\right)\right]. \tag{21}$$

The solution of Eq. (20) is

$$D(u, r) = \frac{1}{k_{\mathrm{B}} T v} \int_u^{\infty} \mathrm{d}u'\, f(u', r)\, \mathrm{e}^{-(u'^2 - u^2)/2k_{\mathrm{B}}Tv} \tag{22}$$

for $v \neq 0$ (Itô and Stratonovich case) and

$$D(u,r) = f(u,r)/u \tag{23}$$

for $v = 0$ (Hänggi-Klimontovich case). We note that (22) reduces to (23) in the special case of additive noise with $f(u, r) \propto u$.

The probability currents (18) and (19) correspond to the following random force and torque terms in the stochastic differential equations of motion:

$$\boldsymbol{F}^{\mathrm{R}}_{ik} = -\boldsymbol{F}^{\mathrm{R}}_{ki} = \sqrt{D(u^{\perp}_{ik}, r_{ik})}\left[\boldsymbol{P}(\widehat{\boldsymbol{r}}_{ik})\boldsymbol{\xi}^{\mathrm{f}}_{ik} - \widehat{\boldsymbol{r}}_{ik}\times\boldsymbol{N}^{\mathrm{f}}_{ik}\right], \tag{24}$$

$$\frac{\boldsymbol{\tau}^{\mathrm{R}}_{ik}}{R_i} = \frac{\boldsymbol{\tau}^{\mathrm{R}}_{ki}}{R_k} = \sqrt{D(u^{\perp}_{ik}, r_{ik})}\left[\widehat{\boldsymbol{r}}_{ik}\times\boldsymbol{\xi}^{\mathrm{f}}_{ik} + \boldsymbol{P}(\boldsymbol{e}_{ik})\boldsymbol{N}^{\mathrm{f}}_{ik}\right], \tag{25}$$

where $\boldsymbol{\xi}^{\mathrm{f}}_{ik}$ and $\boldsymbol{N}^{\mathrm{f}}_{ik}$ are three-dimensional Gaussian white noise vectors with correlations

$$\langle \boldsymbol{\xi}^{\mathrm{f}}_{ij}(t)\boldsymbol{\xi}^{\mathrm{f}}_{kl}(t')\rangle = k_{\mathrm{B}}T\,\boldsymbol{1}\,(\delta_{ik}\delta_{jl} - \delta_{il}\delta_{jk})\,\delta(t-t') \tag{26}$$

$$\langle \boldsymbol{N}^{\mathrm{f}}_{ij}(t)\boldsymbol{N}^{\mathrm{f}}_{kl}(t')\rangle = k_{\mathrm{B}}T\,\boldsymbol{1}\,(\delta_{ik}\delta_{jl} + \delta_{il}\delta_{jk})\,\delta(t-t'). \tag{27}$$

A derivation of these expressions is provided in Section "Methods", Subsection "Theory".

Specific examples of friction types. We will now discuss three particularly interesting choices of amplitude functions $f(u, r)$. The first choice is the *linear friction* model:

$$f_{\mathrm{l}}(u,r) = w(r)\,\gamma_{\mathrm{f}}\,u, \tag{28}$$

where the friction force depends linearly on the relative tangential velocity with a distance-dependent factor $w(r)$ and a global linear friction coefficient γ_{f}. The integral (22) then simply gives

$$D_{\mathrm{l}}(u,r) = w(r)\,\gamma_{\mathrm{f}} \tag{29}$$

and the noise is additive as discussed above. In the linear case, the combined deterministic friction and stochastic forces can be seen as complicated dissipative particle dynamics (DPD) thermostat[39], which extends a transverse DPD thermostat[40] by terms that couple the rotation and translation of particles. This thermostat has already been proposed by Español in the context of fluid particle hydrodynamics[41].

The second interesting choice is the *constant friction* or *Coulomb friction* model:[4]

$$f_{\mathrm{c}}(u,r) = w(r)\,\kappa_{\mathrm{f}}. \tag{30}$$

Here, the friction force only depends on the distance of the particles with a prefactor κ_{f}. This results in multiplicative noise, with the squared amplitude having the form of a complementary error function, which can be evaluated very efficiently in numerical applications:

$$D_{\mathrm{c}}(u,r) = \frac{w(r)\kappa_{\mathrm{f}}\sqrt{\pi}}{\sqrt{2k_{\mathrm{B}}Tv}}\,\mathrm{e}^{\frac{u^2}{2k_{\mathrm{B}}Tv}}\,\mathrm{Erfc}\left(\frac{u}{\sqrt{2k_{\mathrm{B}}Tv}}\right) \tag{31}$$

This model works well in practice as we shall show below, but it has the conceptual problem that the friction force does not have a well-defined limit at $u \to 0^{\pm}$, and may rapidly oscillate between finite positive and negative forces for small tangential velocities.

The third example, the *Coulomb-Newton friction* model avoids this problem and is popular in granular matter models[4]:

$$f_{\mathrm{CN}}(u,r) = \min\left[\gamma_{\mathrm{f}}\,u, w(r)\,\kappa_{\mathrm{f}}\right] \tag{32}$$

In this case, the function $D_{\mathrm{CN}}(u,r)$ is given by

$$D_{\mathrm{CN}}(u,r) = \begin{cases} \frac{w(r)\kappa_{\mathrm{f}}\sqrt{\pi}}{\sqrt{2k_{\mathrm{B}}Tv}}\,\mathrm{e}^{\frac{u^2}{2k_{\mathrm{B}}Tv}}\,\mathrm{Erfc}\left(\frac{u}{\sqrt{2k_{\mathrm{B}}Tv}}\right) & : u \geq \frac{w(r)\kappa_{\mathrm{f}}}{\gamma_{\mathrm{f}}} \\ \gamma_{\mathrm{f}}\left(1 - \mathrm{e}^{\left(u^2 - \left(\frac{w(r)\kappa_{\mathrm{f}}}{\gamma_{\mathrm{f}}}\right)^2\right)/2k_{\mathrm{B}}Tv}\right) & \\ \quad + \frac{w(r)\kappa_{\mathrm{f}}\sqrt{\pi}}{\sqrt{2k_{\mathrm{B}}Tv}}\,\mathrm{e}^{\frac{u^2}{2k_{\mathrm{B}}Tv}}\,\mathrm{Erfc}\left(\frac{w(r)\kappa_{\mathrm{f}}/\gamma_{\mathrm{f}}}{\sqrt{2k_{\mathrm{B}}Tv}}\right) & : u < \frac{w(r)\kappa_{\mathrm{f}}}{\gamma_{\mathrm{f}}} \end{cases} \tag{33}$$

In all three examples, $w(r)$ is a smooth function of the center-to-center distance between the particles i, and k, which ensures that the friction vanishes if the particles are far apart. In the classical Coulomb friction model, the tangential friction force is assumed to be proportional to the normal (repulsive) conservative force between the particles. In the applications shown below, we will consider particles that interact via a purely repulsive Weeks-Chandler-Anderson (WCA) potential[42],

$$U_{\mathrm{WCA}}(r) = \begin{cases} 4\epsilon\left[\left(\frac{\sigma}{r}\right)^{12} - \left(\frac{\sigma}{r}\right)^{6}\right] + \epsilon & , r \leq \sqrt[6]{2}\sigma \\ 0 & , r > \sqrt[6]{2}\sigma. \end{cases} \tag{34}$$

Therefore, adopting the Coulomb friction Ansatz, we will choose $w(r) = -\,\mathrm{d}U_{\mathrm{WCA}}(r)/\mathrm{d}r$.

To validate our approach, we have performed three-dimensional simulations of systems of identical passive colloids interacting with repulsive WCA interactions and frictional contact interactions of the Coulomb-Newton type (with $R = \sigma/2$ and $k_{\mathrm{B}}T = \epsilon$). No additional thermostat is applied. We use a simple Euler-forward scheme to integrate over stochastic forces, corresponding to an implementation of Itô calculus. Figure S2 shows the resulting distributions of the speeds and angular speeds of particles. They are in perfect agreement with the Maxwell-Boltzmann distribution.

Application examples

In the following, we investigate the effect of frictional contact forces in three different systems: In the first subsection below, we simulate simple passive fluids to demonstrate the thermodynamic inconsistencies that arise if only the deterministic frictional contact forces are included in a model. In the second subsection, we consider pressure-driven Poiseuille flows in a slit channel and investigate the coupling of velocity and angular velocity gradients due to frictional contacts in such channels. Furthermore, we use the flow profiles to determine the dynamic viscosity arising from frictional contact interactions. In the last subsection, we study the influence of frictional contacts on motility-induced phase separation (MIPS) in systems of active particles.

All particles have identical masses m, radii $R = \sigma/2$, and moments of inertia $\boldsymbol{I} = \frac{2}{5}mR^2\boldsymbol{1}$, interact with WCA interactions (Eq. (34)), and may be coupled to a medium at rest. The basic equations of motion read

$$m\dot{\boldsymbol{v}}_i = \boldsymbol{F}^{\mathrm{ne}}_i - \gamma\boldsymbol{v}_i + \boldsymbol{\xi}^{\mathrm{s}}_i + \sum_{k\neq i}(-\nabla_i U_{\mathrm{WCA}}(r_{ik}) + \boldsymbol{F}^{\mathrm{f}}_{ik} + \boldsymbol{F}^{\mathrm{R}}_{ik}) \tag{35}$$

$$\frac{\mathrm{d}}{\mathrm{d}t}(\boldsymbol{I}\,\boldsymbol{\omega}_i) = \boldsymbol{\tau}^{\mathrm{ne}}_i - \gamma_{\mathrm{R}}\boldsymbol{\omega}_i + \boldsymbol{N}^{\mathrm{s}}_i + \sum_{k\neq i}(\boldsymbol{\tau}^{\mathrm{f}}_{ik} + \boldsymbol{\tau}^{\mathrm{R}}_{ik}) \tag{36}$$

$$\dot{\boldsymbol{e}}^{(\alpha)}_i = \boldsymbol{\omega}_i \times \boldsymbol{e}^{(\alpha)}_i \text{ for } \alpha = 1, 2 \tag{37}$$

$$\dot{\boldsymbol{r}}_i = \boldsymbol{v}_i \tag{38}$$

where γ and γ_R are translational and rotational friction coefficients describing the interaction with the medium, and the forces $\boldsymbol{\xi}_i^s$ and torques $\boldsymbol{N}_i^s$ are uncorrelated Gaussian white noise terms with zero mean and variance

$$\langle \boldsymbol{\xi}_i^s(t)\boldsymbol{\xi}_k^s(t')\rangle = 2k_BT\,\gamma\,\mathbf{1}\,\delta_{ik}\,\delta(t-t') \tag{39}$$

$$\langle \boldsymbol{N}_i^s(t)\boldsymbol{N}_k^s(t')\rangle = 2k_BT\,\gamma_R\,\mathbf{1}\,\delta_{ik}\,\delta(t-t'), \tag{40}$$

The forces $\boldsymbol{F}_{ik}^{f/R}$ and torques $\boldsymbol{\tau}_{ik}^{f/R}$ model interparticle frictional contacts and as described in the previous section. Additional forces $\boldsymbol{F}_i^{ne}$ and torques $\boldsymbol{\tau}_i^{ne}$ may drive the system out of equilibrium. All densities are expressed by the area fraction $\rho_{area} = \pi NR^2/A$, the volume fraction $\rho_{volume} = 4\pi NR^3/3V$, or the number density $n = N/A$, where N is the number of particles, and A, V are the area and the volume. In two-dimensional systems, the position of the particles is restricted to a plane.

All quantities will be given in units of the length σ, the thermal energy k_BT, and a "natural" time unit t_0, which is specified for each case study, along with other simulation parameters, in the Methods section.

Thermodynamic consistency in models with frictional contact interactions. Above (see Eq. (9)), we have shown that dissipative frictional forces necessarily reduce the kinetic energy of colliding particles, but combined dissipative and stochastic frictional forces constitute a valid thermostat in simulations of passive colloidal systems (see Supplementary Note 2 with Fig. S2). When considering systems of particles in an implicit medium as in Eqs. (35) and (36), one might be tempted to omit the stochastic force and torque terms, $\boldsymbol{F}_{ik}^R$ and $\boldsymbol{\tau}_{ik}^R$, assuming that the coupling to a bath medium (i.e., the corresponding Langevin thermostat) is sufficient to guarantee sampling of a canonical ensemble in the absence of nonequilibrium forces $\boldsymbol{F}_i^{ne}$. In the following, we will demonstrate that this assumption is not correct, and that the stochastic frictional contact terms must necessarily be included to avoid thermodynamic inconsistencies.

For this purpose, we have investigated two and three-dimensional systems of passive particles with frictional contact interactions, which are coupled to a bath medium as described above. The nonequilibrium forces and torques were set to zero, $\boldsymbol{F}_i^{ne} = \boldsymbol{\tau}_i^{ne} = 0$. The area fraction of the two-dimensional system was chosen $\rho_{area} = 0.6$ and the volume fraction of the three-dimensional system $\rho_{volume} = 0.3$. All systems contain $N = 10\,000$ particles with periodic boundary conditions in all directions. We performed simulations for the friction types linear, Coulomb and Coulomb-Newton. Each type was simulated twice, once without stochastic friction $\boldsymbol{F}_{ik}^R$ and torques $\boldsymbol{\tau}_{ik}^R$ and once including them. The systems were equilibrated over a time 20 t_0 using a time step of $\Delta t = 0.001\ t_0$ for the linear and Coulomb-Newton friction model and $\Delta t = 0.0001\ t_0$ for the Coulomb friction model. The data were then collected over a simulation time period of 200 t_0. The distributions of speeds and angular speeds were then compared to the theoretically expected Maxwell-Boltzmann distributions at the bath temperature k_BT.

Figure 2 depicts such a comparison for a two-dimensional system with frictional contacts according to the Coulomb friction model and different values of κ_f. Corresponding figures for other types of friction and in three dimensions are provided in supplemental information (Supplementary Note 3 with Figs. S3 and S4). When omitting the stochastic contact forces and torques in the simulations (star symbols), the speed and angular speed distributions clearly deviate from the theoretically expected Maxwell-Boltzmann distribution $P_{2D,v}$ and $P_{2D,\omega}$, which is shown as dashed black line. The distribution is shifted to the left, such that smaller speeds are overrepresented and larger ones are underrepresented, indicating that the Langevin thermostat is not able to fully compensate the loss of kinetic energy due to frictional forces during collisions. However, when the stochastic contact terms are included, the simulation data (circles) coincide with the expectation.

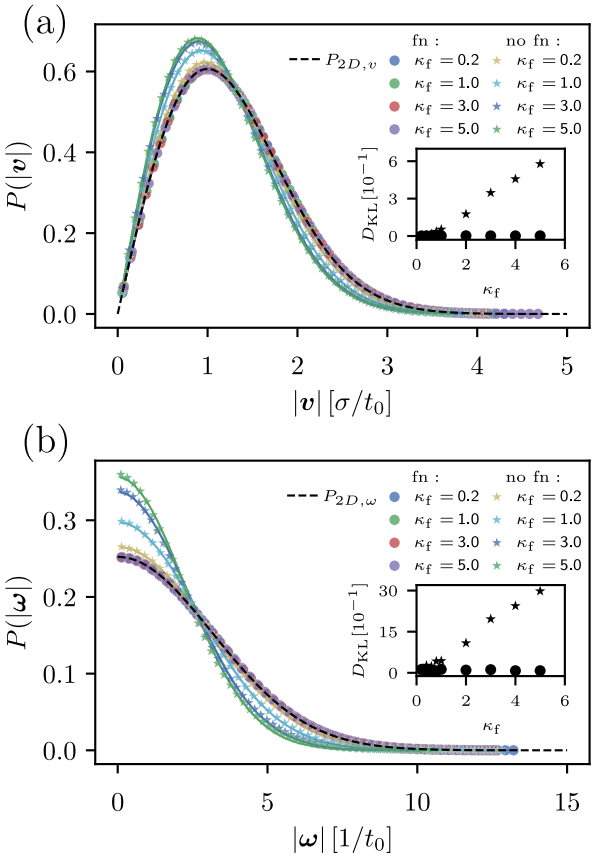

Fig. 2 | Speed distributions showing that incomplete frictional noise violates equipartition. Speed histograms $P(|\boldsymbol{v}|)$ (**a**) and $P(|\boldsymbol{\omega}|)$ (**b**) of the absolute translational velocity $|\boldsymbol{v}|$ (in units of σ/t_0) and absolute angular velocity $|\boldsymbol{\omega}|$ (in units of $1/t_0$) for a two-dimensional passive colloid system with frictional contact interactions according to the Coulomb friction model, Eq. (30), and for different friction constants κ_f as indicated. Stars (labeled "no fn") show data from simulations without stochastic contact friction terms, circles (labeled "fn") correspond to the full model including frictional noise. Solid colored lines are fits to appropriate Maxwell-Boltzmann distribution with fitted effective temperature, T_{eff}; the black dashed line shows the theoretical expectation for $k_BT_{eff} = k_BT$. Insets display the corresponding Kullback-Leibler divergence between the distribution measured in simulations and the fitted Maxwell-Boltzmann distribution.

One might argue that the main effect of omitting the stochastic contact terms is to reduce the kinetic temperature of the particles, but that the system might still adopt an "equilibrium" state corresponding to such a reduced temperature. However, a closer look at the data shows that this is not the case. First, we can determine the "effective" temperature T_{eff} by fitting the speed and angular speed histograms to the Maxwell-Boltzmann distribution, using T_{eff} as fit parameter. The result is shown in Fig. 3 for two- and three-dimensional systems, three different types of contact friction, and varying friction parameters. Not surprisingly, the effective temperature decreases with increasing friction parameters. More importantly, however, the effective kinetic temperature obtained from the speed histogram and the angular speed histogram differ from each other. This clearly indicates that the system cannot be mapped to an equilibrium system.

A second, more subtle nonequilibrium signature is that the shape of the distribution also differs from the expected Maxwell-Boltzmann shape. To quantify this, we have calculated the Kullback-Leibler divergence, D_{KL}, between the real (simulated) histograms and the fitted histograms with shifted effective temperature:

$$D_{KL}\left(P_{sim}(\boldsymbol{x})||P_{fit}(\boldsymbol{x})\right) = \int \mathrm{d}\boldsymbol{x}\, P_{sim}(\boldsymbol{x}) \ln\left(\frac{P_{sim}(\boldsymbol{x})}{P_{fit}(\boldsymbol{x})}\right), \tag{41}$$

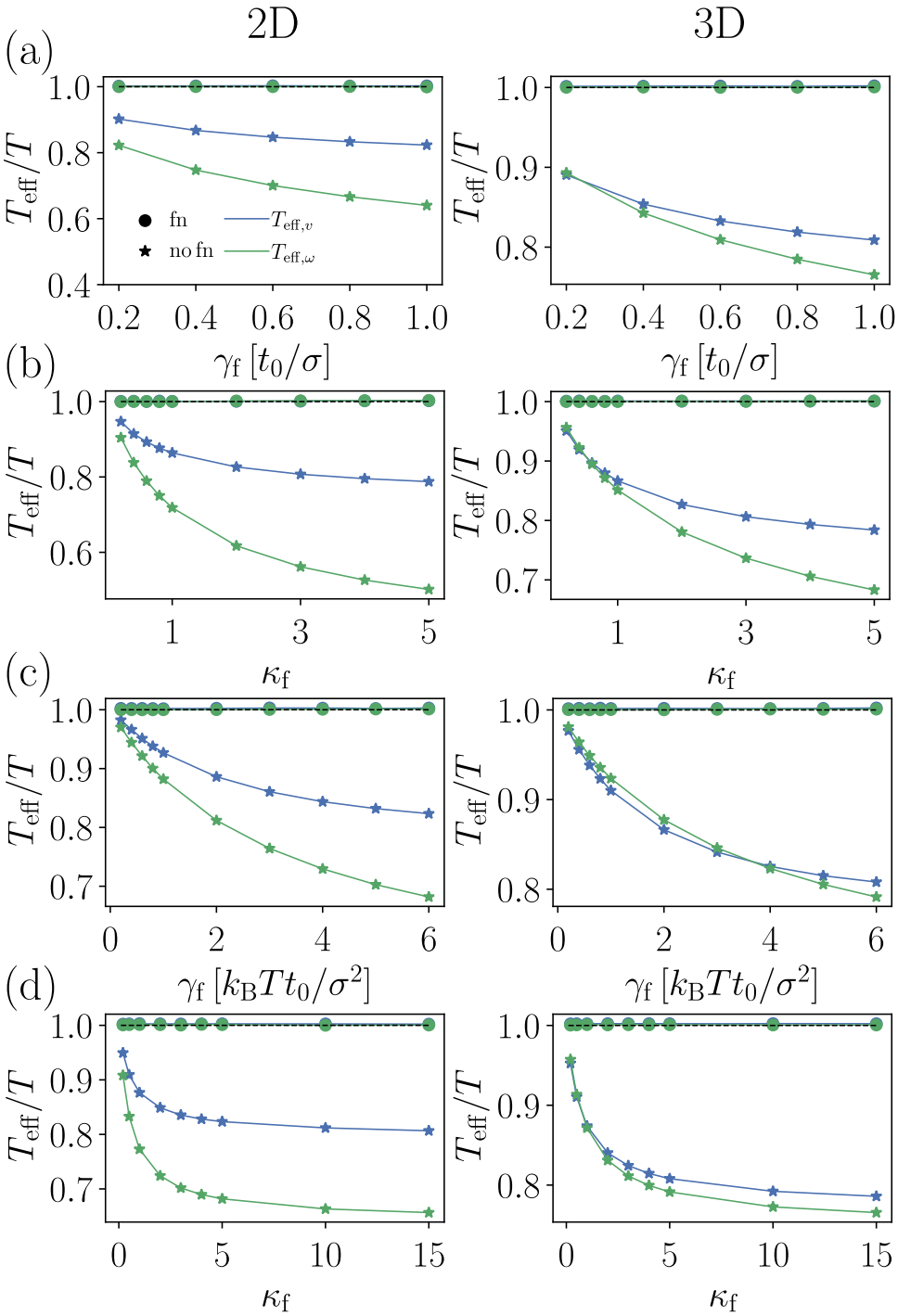

Fig. 3 | Impact of inconsistent frictional noise on effective kinetic temperatures. Ratio of effective kinetic temperatures T_{eff} to the imposed temperature T obtained by fitting translational speed (green) and angular speed (blue) histograms to the corresponding Maxwell-Boltzmann distributions. Results are shown for simulations without (stars) and with (circles) stochastic contact friction terms, in two-dimensional (i) and three dimensional (ii) systems, and for different friction models: (**a**) linear friction, (**b**) Coulomb friction, Coulomb-Newton friction with (**c**) fixed friction constant $\kappa_{\mathrm{f}} = 5$ and varying linear friction parameter γ_{f}, and (**d**) fixed $\gamma_{\mathrm{f}} = 6\,k_{\mathrm{B}}Tt_0/\sigma^2$ and varying κ_{f}. Error bars are smaller than symbol size.

where $\boldsymbol{x}$ stands for $\boldsymbol{v}$ or $\boldsymbol{\omega}$, $P_{\mathrm{sim}}(\boldsymbol{x})$ is the distribution from simulation, and $P_{\mathrm{fit}}(\boldsymbol{x})$ the fitted distribution. The results for the Coulomb friction model are shown in the insets of Fig. 2. If the stochastic contact terms are omitted in the simulation, the Kullback-Leibler divergence deviates from zero for large friction parameters, indicating that the shape of the distribution from the simulations deviates from the fitted Maxwell-Boltzmann distribution. If the stochastic terms are included, the Kullback-Leibler divergence is zero, hence the simulations produce the correct distribution functions.

Pressure-driven flows. Next, we study the rheological properties of fluids of repulsive particles with frictional surface interactions. Since individual particles are not coupled to a substrate, the parameters γ and γ_{R} in Eqs. (35), (36) are set to zero. Also, solvent-mediated hydrodynamic interactions between particles are neglected[43]. However, the particles may still interact with confining walls. This model describes, e.g., colloidal suspensions in a regime where the total shear viscosity is dominated by particle-particle interactions rather than particle-solvent friction. We consider a Poiseuille flow in a slit channel geometry. The nonequilibrium forces are set to $\boldsymbol{F}_i^{\mathrm{ne}} \equiv F\,\boldsymbol{e}_x$, i.e., all particles are subject to a constant bulk force in the x direction. Such a setup is commonly used to mimic pressure-driven flows[44] in a pressure gradient $\mathrm{d}P/\mathrm{d}x = -F\,n$, where n is the local number density of particles. The particles are confined by two identical walls, consisting of a layer of virtually immobilized particles j (mass $10^{10}\,m$) with diameter σ and y-coordinates

$$y_j = \pm 8.5847\sigma + \delta_{\mathrm{w}}\,\zeta_j, \tag{42}$$

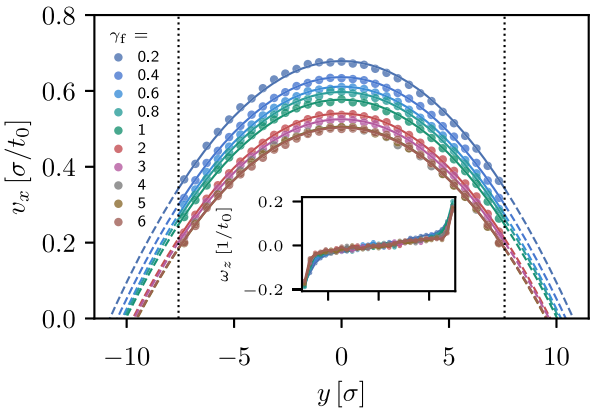

Fig. 4 | Poiseuille flow profiles of frictional contact fluids. Examples of velocity profiles $v_x(y)$ (in units of σ/t_0) as a function of the y coordinate (in units of σ) for fluids with Coulomb-Newton-type frictional contact interactions. The friction constant is $\kappa_f = 5$, while the linear friction parameter γ_f varies in the range 0.2-6 k_BTt_0/σ^2, as indicated in the legend (different values of γ_f correspond to different colors). The fluids are confined between walls with roughness parameter $\delta_w = 0$ (see text) and are subject to a bulk force $F = 0.01\ k_BT/\sigma$. Solid lines show fits to parabolic profile. The inset shows the corresponding profiles of the z-component of the angular velocity, ω_z, in units of $1/t_0$. Error bars are smaller than system size.

which are arranged on a square lattice with lattice constant $a = \sigma$ in the (xz)-plane. In Eq. (42), ζ_j denotes uncorrelated random numbers that are drawn from a Gaussian distribution with mean zero and variance 1, and the parameter $\delta_w > 0$ allows to tune the degree of surface roughness. For technical reasons, the random numbers are the same on both sides of the slab. All particles, mobile and immobile, interact via repulsive WCA interactions and frictional contact interactions of the Coulomb-Newton type (Eq. (32)). We considered systems of 10000 particles at volume fraction $\rho_{\text{volume}} = 0.15$ in a simulation box with accessible volume $V = (151.694 \times 15.1694 \times 15.1694)\sigma^3$, and periodic boundary conditions in the x and z directions. The time step in the simulations was $\Delta t = 0.001\ t_0$. After initialization, each system was simulated over a time of 500 t_0, which was sufficient to reach a stationary state (Supplementary Note 4 with Fig. S5). Data were then collected over a simulation time period of 6000 t_0. In the following, we will show data obtained for bulk forces $F = 0.01\ k_BT/\sigma$. We have also simulated systems at $F = 0.02\ k_BT/\sigma$ and verified that the velocity and angular velocity profiles are proportional to F as expected in the linear regime.

Figure 4 (main figure) shows examples of resulting velocity profiles for different thermostat parameters γ_f at roughness parameter $\delta_w = 0$. They have the parabolic shape expected for Poiseuille flow of Newtonian fluids, if one allows for substantial slip at the surface. Compared to regular DPD simulations of Poiseuille flow, in our system, slip is facilitated by the possibility that particles roll off on the surface without dissipating energy due to friction. This rolling involves a collective rotational motion to the particles, which however quickly decreases further away from the surface. More generally, the inset of Fig. 4 (main figure) demonstrates that shear in the velocity profiles ($dv_x/dv_y \neq 0$) induces rotational motion of particles in the fluid.

Fitting the velocity profiles in Fig. 4 to the prediction of the Stokes equation for a fluid with volume fraction ρ_{volume}, and partial slip boundary conditions $(v_x(y_B)/v_x'(y_B) = \delta_B$, where δ_B is the slip length, and y_B the position of the hydrodynamic boundary)

$$v_x(y) = -\frac{3\rho_{\text{volume}}}{\pi\eta} F(y^2 - y_0^2), \tag{43}$$

we can extract the dynamic viscosity η and the zero crossing parameter $y_0 = (\delta_B + y_B)^2 - \delta_B^2$. The parameters δ and y_B can be disentangled following a procedure proposed by Allen[45], which is based on the comparison of Poiseuille flow profiles and complementary Couette flow profiles. To apply it, we performed additional simulations with a slightly altered setup. We removed the constant bulk force and slid the walls in opposite $x-$ directions at a constant velocity $v_{\text{wall}} = \pm\ 1\ \sigma/t_0$, which yielded linear velocity profiles (see Supplementary Note 5 with Fig. S6). Then we determined the distance C between the two points where the extrapolated linear profile equals the wall velocity. From this we can determine the squared slip length via $\delta_B^2 = C^2/4 - {y_0}^2$ and the distance between the physical and the hydrodynamic boundary as $y_B = \delta_B - (C - 15.1694)/2$.

The results of such fits are shown in Fig. 5. The distance between the physical and the hydrodynamic boundary y_B equals zero (within the error), compatible with findings from previous studies of simple fluids at hard walls[45,46]. The dynamic shear viscosity of the fluid only slightly increases with the friction parameter γ_f and is independent of the parameter κ_f, indicating that, at this volume fraction, the shear viscosity is basically determined by the conservative interactions between the particles. In contrast, the contact friction does influence the surface slip: The stronger the contact friction interactions, the smaller the slip length. Nevertheless, it seems difficult to achieve zero slip length in this system due to the possibility that particles can roll off at the surface. The slip length is roughly independent of the roughness parameter δ_w up to $\delta_w \sim 0.1$ and then decreases as δ_w is increased further

For comparison, we have also studied the effect of turning off the frictional contact noise. The results are shown in Supplementary Note 6 with Fig. S7. In the absence of thermal noise, the viscosity drops roughly by a factor of 5, and likewise, the surface slip increases dramatically. Hence thermal noise significantly enhances the energy dissipation in the fluid. The reason is that particles in noiseless fluids almost stop moving perpendicular to the bulk force or sliding walls, resulting in fewer particle collisions and fewer frictional contacts.

Even though our results so far suggest that the flow profiles can be described by the Stokes equation, the relatively strong coupling to angular rotation motion suggests that nonlinear rheological effects might be important in fluids involving frictional contact interactions. Unfortunately, increasing the driving force F and pushing it into the nonlinear regime mainly has the effect of increasing the slip length, such that the flow profiles become plug like. In order to avoid this effect and investigate the coupling between shear rate and rotational motion of particles at higher shear rates, we have used an artificial simulation setup which is popular in rheological simulation studies of complex fluids[47,48]: We apply periodic boundary conditions in *all* directions, but split the simulation box in half in the y direction and impose opposing bulk forces in both halves: $\boldsymbol{F}_i^{\text{ne}} = F\,\boldsymbol{e}_x$ for $y_i > 0$, and $\boldsymbol{F}_i^{\text{ne}} = -F\,\boldsymbol{e}_x$ for $y_i < 0$. According to the Stokes equation, this should result in a sequence of two parabolic flow profiles in opposite directions. In our simulations, we found that, instead, vortices developed in the high shear regions at higher forces bulk forces, which eventually destroyed the stationary Poiseuille-like flow profiles. An example for $F = 0.5\ k_BT/\sigma$ is provided in Supplementary Movie 1. The formation of these vortices was prevented in the presence of solid walls. Nevertheless, our results suggest that the linear response regime in fluids with frictional contact interactions is small and that their dynamic behavior might often be dominated by nonlinear effects.

Active particles and motility-induced phase separation. As a final example, we consider the effect of frictional contact interactions on structure formation in systems of active particles. Specifically, we focus on the phenomenon of motility-induced phase separation (MIPS)[49], which has been observed both in systems of active Brownian particles (ABPs) and active Langevin particles (ALPs). ALPs follow the equations of motion (Eqs. (35)–(38)) with effective active force $\boldsymbol{F}_i^{\text{ne}} = F_0\boldsymbol{e}_i^{(1)}$ (and originally without frictional contact terms)[50]. ABPs obey the same equations of motion as ALPs in the overdamped limit (Eqs. (35)–(38) with $m \to 0$ and $\boldsymbol{I} \to 0$). In a certain parameter range, the effective active force can induce phase separation between coexisting dense and dilute regimes even in the absence of attractive conservative forces between particles. The reason is, loosely speaking, that particles which happen to

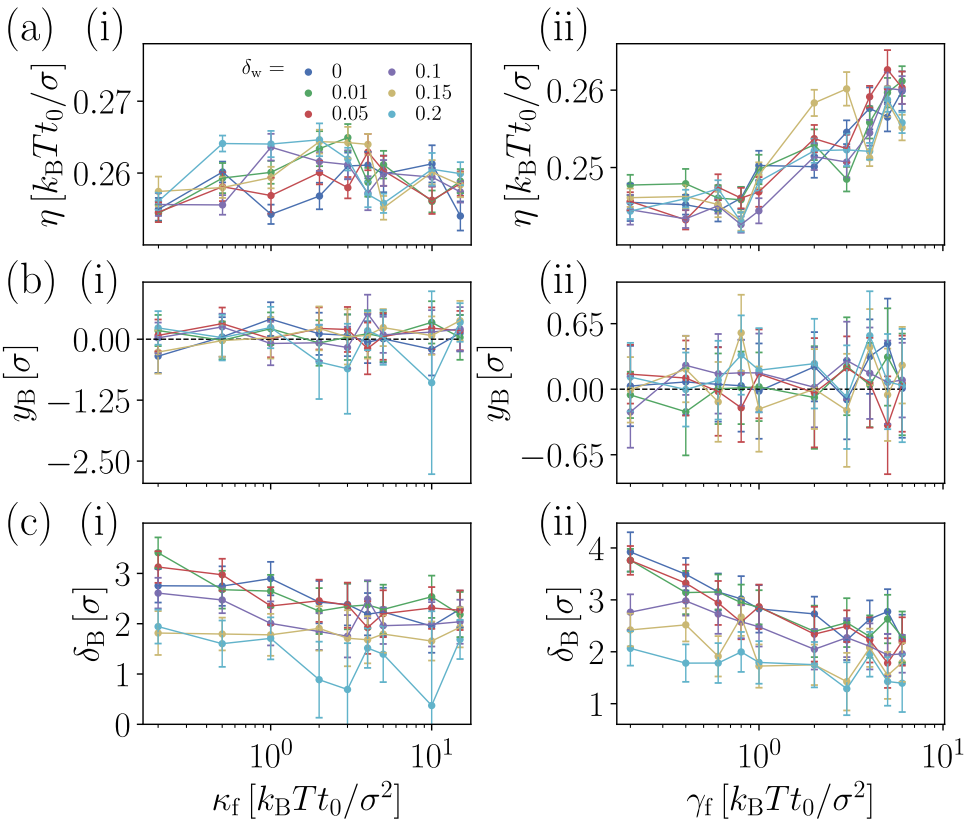

Fig. 5 | Rheological properties of frictional contact fluids. Dynamic viscosity η in units of k_BTt_0/σ (**a**), distance between the hydrodynamic and physical boundaries y_B (in units of σ) (**b**), and slip length δ_B (in units of σ) (**c**), obtained from parametric fits to Poiseuille flow and Couette flow simulation profiles (see Fig. 4 and Fig. S6) for fluids with Coulomb-Newton-type frictional contact interactions in slit geometry. Results are shown for various values of the surface roughness parameter δ_w, (differently colored symbol; see legend of (**a**.i)), as functions of (i) the friction parameter κ_f with fixed $\gamma_f = 6\ k_BTt_0/\sigma^2$, and (ii) γ_f with fixed $\kappa_f = 5$. Error bars represent one-standard-deviation uncertainties of the fitted parameters.

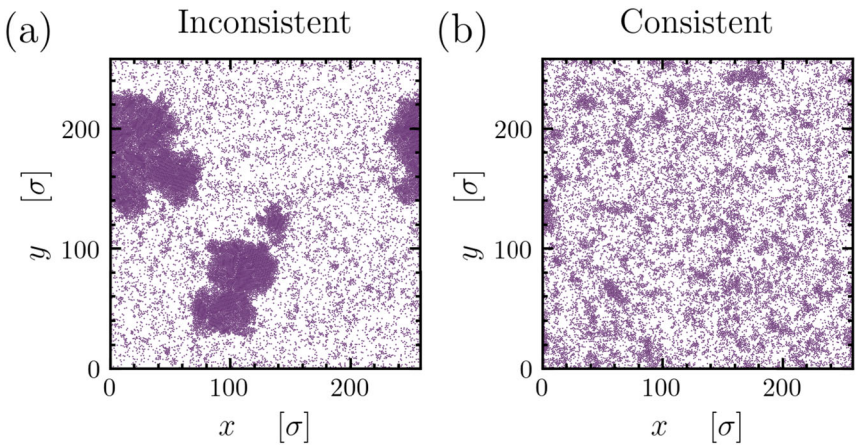

Fig. 6 | Impact of noise (in)consistency on motility induced phase separation (MIPS) of active Langevin particles (ALPs). Snapshots from simulations of 20000 ALPs at active Force $F_0 = 25k_BT/\sigma$ and number density $n = 0.3/\sigma^2$ after equilibration with Coulomb-Newton friction. **a** Thermodynamically inconsistent treatment of the frictional contacts, i.e., friction without the corresponding stochastic noise. **b** Thermodynamically consistent treatment including both friction and its associated noise. MIPS is observed in the inconsistent treatment (**a**), whereas no MIPS is observed in the consistent case (**b**).

push against each other by the active forces remain stuck to each other for some time before they reorient. If other particles collide with the stuck particle assembly before the particles reorient, the clusters tend to grow until the system is phase separated. Roughly, this happens at sufficiently high active particle speeds and densities, such that the collision rate is higher than the reorientation rate. Frictional contact forces can enhance particle aggregation, as two particles with zero or small initial angular velocity that collide off-center (nonzero impact parameter) are forced to rotate in the same direction, causing them to stick together even longer. This effect has recently been reported for systems of ABPs by Nie et al.[25] in a model that accounted for dissipative friction contact forces similar to the Coulomb-Newton type and which is also well-known in the granular community[5]. The model by Nie et al. did not include corresponding stochastic terms with thermodynamically consistent coupling of translational and rotational noise.

In our simulations, we study two-dimensional systems of $N = 20,000$ ALPs with model parameters as specified earlier (beginning of Section "Application examples"), which were chosen in accordance with own previous work on MIPS where we know the parameter regime of the MIPS region[51]. In particular, the mass is set to be $m = 0.05\,k_BT\,(t_R/\sigma)^2$, which is still in the underdamped regime as compared to the overdamped system studied by Nie et al.[25]. We include frictional contact interactions of the Coulomb-Newton type with parameters $\gamma_f = 1\ k_BTt_R/\sigma^2$ and $\kappa_f = 1$. The simulation time step was $\Delta t = 10^{-5}\ t_R$, and periodic boundary conditions were applied in all directions. Neglecting the thermodynamic correction of the frictional contacts can cause the collective behavior to vary significantly. This can be seen in Fig. 6, where the simulation with thermodynamically inconsistent frictional contacts leads to MIPS, whereas the simulation of the consistent treatment shows no MIPS. To explore the importance of a thermodynamically consistent treatment more

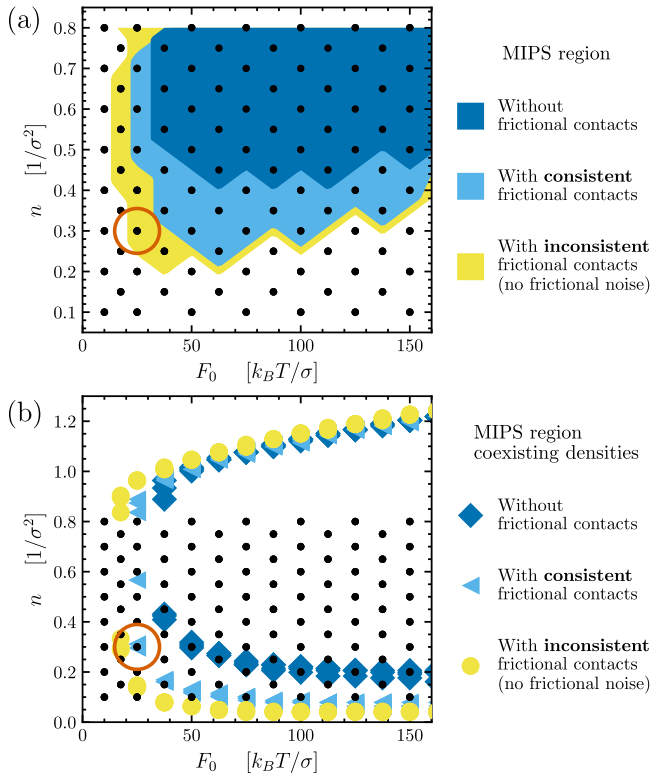

Fig. 7 | Influence of frictional contacts on motility-induced phase separation (MIPS). a MIPS regime in two-dimensional systems of ALPs without frictional contacts (dark blue), with thermodynamically inconsistent frictional contacts (yellow), and with thermodynamically consistent frictional contacts (light blue), as a function of active force F_0 and number density n. Black dots indicate state point simulated, while the colored regions mark where MIPS spontaneously emerges (bimodal density distribution) from a uniform initial state. The red circle indicates the parameters corresponding to the simulation snapshots shown in Fig. 6. **b** Corresponding coexisting densities in the MIPS regime. See text for further explanation and simulation details.

systematically, we now compare the phase diagram for three different cases: (i) without frictional contacts, (ii) with Coulomb-Newton friction with frictional noise, and (iii) with Coulomb-Newton friction, but without frictional noise. MIPS was identified using AMEP[52] by computing the local density on a uniform grid. A bimodal distribution in the resulting density histogram indicates phase separation. The coexisting densities within the MIPS region[53,54] were identified by locating the two peaks in this density histogram (cf. Fig. 7, b).

The resulting non-equilibrium MIPS phase diagrams for systems with and without frictional interactions are shown in Fig. 7(a). It is worth noting that the coexistence densities—which in an equilibrium system would give the binodals of phase separation – do not coincide with the boundaries of the MIPS regime. This discrepancy might be a signature of the system's nonequilibrium nature or may arise from strong finite-size effects in the simulations.

As reported by Nie et al.[25] for ABPs, the contact friction forces significantly expand the regime in which MIPS is observed. This can also be seen in the case of the inertial ALPs we investigated. More importantly, the comparison between the thermodynamically consistent case (with frictional noise) and the thermodynamically inconsistent case (no frictional noise) shows a notable difference in the morphology of the MIPS phase diagram. This demonstrates that neglecting frictional noise, despite altering the equilibrium distribution of colloidal particles only relatively mildly, can lead to a wrong prediction for the collective behavior of a nonequilibrium many particle system in certain parameter regimes.

Conclusions

We have constructed a thermodynamically consistent way of modeling thermal fluctuations in particle models with frictional contact interactions. Our approach is based on the construction of appropriate Fokker-Planck equations for such systems under the constraint that the stationary solution for equilibrium systems should be the Boltzmann distribution function. Importantly, it shows that coupled frictional forces and torques arising from frictional contacts must necessarily be accompanied by stochastic forces and torques that are coupled in a structurally similar manner. We have demonstrated that neglecting such stochastic terms in equilibrium simulations results in stationary distributions that differ from the Boltzmann distribution, both regarding effective temperature and shapes of the distribution. Even more seriously, effective temperatures related to different degrees of freedom, such as momenta and angular momenta, are no longer equal if the stochastic forces and torques are not modeled consistently.

We have considered a general form of frictional contact interactions, which is inspired by models for granular matter. In general, the resulting stochastic terms depend on the velocities and angular velocities of particles and are therefore instances of multiplicative noise. Hence, we have separately considered three popular choices of stochastic calculus, Itô, Stratonovich, and Hänggi-Klimontovich, and we have provided explicit expressions for the stochastic Langevin noise terms for all three choices. Then we have validated the approach with simulations based on the Itô calculus and presented applications to driven flows and active particles undergoing MIPS.

In driven flows, we have seen that frictional contacts lead to a coupling of rotational and translational degrees of freedom, which may lead to nonlinear effects already at low driving forces. At surfaces, particles can roll off, facilitating slip. More generally, the interplay of rolling and sliding friction may give rise to interesting structures at high shear rates, which we will explore in future work.

In the case of MIPS, we have recovered the result of a previous study[25] that frictional contacts increase the width of the phase-separated region. Beyond that, we have shown that thermodynamic inconsistencies can lead to a wrong prediction of the resulting collective behavior, in parameter regimes near the transition line between the uniform and the MIPS phase. We anticipate that the coupling of rotational and translational noise might be relevant in active chiral matter and unveil new mechanisms of pattern formation.

In future work, it will be interesting to extend our approach to the overdamped case. The present study suggests that also in underdamped models, e.g., for active Brownian particles, the coupling of rotational and translational stochastic terms will be crucial to achieve thermodynamic consistency. Unfortunately, simply taking the limit $m \to 0$ and $\boldsymbol{I} \to 0$ is tricky in the presence of frictional contacts and will require special efforts.

Furthermore, it will be interesting to examine the effect of phenomena that have been neglected in the present work. In our model, we have not included spinning friction, i.e., friction that occurs if two particle faces are rotating against each other. This type of friction is not present in strictly two-dimensional systems, but may become important in three-dimensional or quasi two-dimensional systems of translationally nearly immobile spinning particles. Applying our Fokker-Planck approach to deriving the correct noise structure for this type of friction should be a relatively straightforward exercise. We have also neglected memory effects[4,5], which become important in systems that not only exhibit dynamic friction, but also static friction. Modeling thermal fluctuations consistently in such cases will be an interesting challenge for future work.

Methods

Theory: relation between Langevin equation and the Fokker-Planck equation

We recall the general relation between the Langevin equation and the Fokker-Planck equation for systems with many variables[35]. We consider a system of stochastic differential equations for a vector of N variables, $\boldsymbol{x} = \{x_i\}$

with the Langevin equation

$$\dot{\boldsymbol{x}} = \boldsymbol{\mu}(\boldsymbol{x}, t) + \boldsymbol{\sigma}(\boldsymbol{x}, t)\,\boldsymbol{\eta}(t), \tag{44}$$

where $\boldsymbol{\eta}(t)$ is an uncorrelated Gaussian white noise vector with fluctuations

$$\langle \eta_\alpha(t)\eta_\beta(t')\rangle = \delta_{\alpha\beta}\,\delta(t-t'). \tag{45}$$

Then the corresponding Fokker-Planck equation for the distribution function $P(\boldsymbol{x}, t)$ is

$$\partial_t \mathcal{P} = -\sum_\alpha \partial_\alpha \mu_\alpha(\boldsymbol{x})\,\mathcal{P} - \sum\nolimits_\alpha J^{\mathrm{R}}_\alpha \mathcal{P} \tag{46}$$

with[35,55]

$$J^{\mathrm{R}}_\alpha = -\frac{1}{2}\sum_{\beta,\gamma} \partial_\beta\, \sigma_{\alpha\gamma}(\boldsymbol{x}, t)\sigma_{\beta\gamma}(\boldsymbol{x}, t) \tag{47}$$

in the Itô calculus,

$$J^{\mathrm{R}}_\alpha = -\frac{1}{2}\sum_{\beta,\gamma} \sigma_{\alpha\gamma}(\boldsymbol{x}, t)\,\partial_\beta\, \sigma_{\beta\gamma}(\boldsymbol{x}, t) \tag{48}$$

in the Stratonovich calculus, and

$$J^{\mathrm{R}}_\alpha = -\frac{1}{2}\sum_{\beta,\gamma} \sigma_{\alpha\gamma}(\boldsymbol{x}, t)\,\sigma_{\beta\gamma}(\boldsymbol{x}, t)\,\partial_\beta \tag{49}$$

in the Hänggi-Klimontovich calculus. If $\boldsymbol{\sigma}$ does not depend on $\boldsymbol{x}$ (additive noise), then all formalisms give the same Fokker-Planck equation.

With these general relations in mind, our task is to translate the Fokker-Planck probability operators $\mathbf{J}^{\mathrm{R}}_{ik,\boldsymbol{p}}$ and $\mathbf{J}^{\mathrm{R}}_{ik,\boldsymbol{j}}$, Eqs. (18) and (19), into stochastic force and torque terms in the equations of motion of the particles i and k. In the notation of Eqs. (44)–(49), the sum $[\mathbf{J}^{\mathrm{R}}_{ik,\boldsymbol{p}} + \mathbf{J}^{\mathrm{R}}_{ik,\boldsymbol{j}}]_\alpha$ corresponds to terms $-\frac{1}{2}\sum_{\beta,\gamma}\partial_\beta\sigma^{(ik)}_{\alpha\gamma}\sigma^{(ik)}_{\beta\gamma}$, $-\frac{1}{2}\sum_{\beta,\gamma}\sigma^{(ik)}_{\alpha\gamma}\partial_\beta\sigma^{(ik)}_{\beta\gamma}$, or $-\frac{1}{2}\sum_{\beta,\gamma}\sigma^{(ik)}_{\alpha\gamma}\sigma^{(ik)}_{\beta\gamma}\partial_\beta$, depending on the calculus, where the indices α, β, γ can take 12 values corresponding to the components of the variables $\boldsymbol{p}_i, \boldsymbol{p}_k, \boldsymbol{j}_i, \boldsymbol{j}_k$. We can decompose the matrices $\boldsymbol{\sigma}^{(ik)}$ as $\boldsymbol{\sigma}^{(ik)} = \sqrt{k_{\mathrm{B}}T}D(u^{\perp}_{ik}, r_{ik})\,\widehat{\boldsymbol{\sigma}}^{(ik)}$ with reduced matrices $\widehat{\boldsymbol{\sigma}}(\widehat{\boldsymbol{r}}_{ik})$ that are independent of $\boldsymbol{p}_i, \boldsymbol{p}_k, \boldsymbol{j}_i, \boldsymbol{j}_k$ and satisfy

$$\frac{1}{2}\hat{\boldsymbol{\sigma}}\hat{\boldsymbol{\sigma}}^{\mathrm{T}} = \left(\begin{array}{cc|cc} \boldsymbol{P}(\hat{\boldsymbol{r}}_{ik}) & -\boldsymbol{P}(\hat{\boldsymbol{r}}_{ik}) & -R_i\boldsymbol{A}(\hat{\boldsymbol{r}}_{ik}) & -R_k\boldsymbol{A}(\hat{\boldsymbol{r}}_{ik}) \\ -\boldsymbol{P}(\hat{\boldsymbol{r}}_{ik}) & \boldsymbol{P}(\hat{\boldsymbol{r}}_{ik}) & R_i\boldsymbol{A}(\hat{\boldsymbol{r}}_{ik}) & R_k\boldsymbol{A}(\hat{\boldsymbol{r}}_{ik}) \\ \hline R_i\boldsymbol{A}(\hat{\boldsymbol{r}}_{ik}) & -R_i\boldsymbol{A}(\hat{\boldsymbol{r}}_{ik}) & R_i^2\boldsymbol{P}(\hat{\boldsymbol{r}}_{ik}) & R_iR_k\boldsymbol{P}(\hat{\boldsymbol{r}}_{ik}) \\ R_k\boldsymbol{A}(\hat{\boldsymbol{r}}_{ik}) & -R_k\boldsymbol{A}(\hat{\boldsymbol{r}}_{ik}) & R_iR_k\boldsymbol{P}(\hat{\boldsymbol{r}}_{ik}) & R_k^2\boldsymbol{P}(\hat{\boldsymbol{r}}_{ik}) \end{array}\right).$$

Here $\boldsymbol{A}(\widehat{\boldsymbol{r}}_{ik})$ is defined as the antisymmetric matrix with $\boldsymbol{A}(\widehat{\boldsymbol{r}}_{ik})\boldsymbol{a} = \widehat{\boldsymbol{r}}_{ij} \times \boldsymbol{a}$ for all $\boldsymbol{a}$. One possible solution for $\hat{\boldsymbol{\sigma}}$ is

$$\hat{\boldsymbol{\sigma}} = \left(\begin{array}{cc|cc} \boldsymbol{P}(\hat{\boldsymbol{r}}_{ik}) & 0 & -\boldsymbol{A}(\hat{\boldsymbol{r}}_{ik}) & 0 \\ -\boldsymbol{P}(\hat{\boldsymbol{r}}_{ik}) & 0 & \boldsymbol{A}(\hat{\boldsymbol{r}}_{ik}) & 0 \\ \hline R_i\boldsymbol{A}(\hat{\boldsymbol{r}}_{ik}) & 0 & R_i\boldsymbol{P}(\hat{\boldsymbol{r}}_{ik}) & 0 \\ R_k\boldsymbol{A}(\hat{\boldsymbol{r}}_{ik}) & 0 & R_k\boldsymbol{P}(\hat{\boldsymbol{r}}_{ik}) & 0 \end{array}\right).$$

This can be checked using the relations

$$\boldsymbol{P}(\widehat{\boldsymbol{r}}_{ik})\boldsymbol{P}(\widehat{\boldsymbol{r}}_{ik})^{\mathrm{T}} = \boldsymbol{A}(\widehat{\boldsymbol{r}}_{ik})\boldsymbol{A}(\widehat{\boldsymbol{r}}_{ik})^{\mathrm{T}} = \boldsymbol{P}(\widehat{\boldsymbol{r}}_{ik})$$
$$\boldsymbol{A}(\widehat{\boldsymbol{r}}_{ik})\boldsymbol{P}(\widehat{\boldsymbol{r}}_{ik})^{\mathrm{T}} = -\boldsymbol{P}(\widehat{\boldsymbol{r}}_{ik})\boldsymbol{A}(\widehat{\boldsymbol{r}}_{ik})^{\mathrm{T}} = \boldsymbol{A}(\widehat{\boldsymbol{r}}_{ik}).$$

With this choice of $\widehat{\boldsymbol{\sigma}}$, half of the Gaussian random variables η_i actually do not enter the Langevin equations of motion and can be omitted. We denote the other half as $\boldsymbol{\xi}^{\mathrm{f}}_{ij} = -\boldsymbol{\xi}^{\mathrm{f}}_{ji}$ and $\boldsymbol{N}^{\mathrm{f}}_{ij} = \boldsymbol{N}^{\mathrm{f}}_{ji}$ and require them to be three-dimensional Gaussian white noise vectors with correlations

$$\langle \boldsymbol{\xi}^{\mathrm{f}}_{ij}(t)\boldsymbol{\xi}^{\mathrm{f}}_{kl}(t')\rangle = k_{\mathrm{B}}T\,\boldsymbol{1}\,(\delta_{ik}\delta_{jl} - \delta_{il}\delta_{jk})\,\delta(t-t')$$
$$\langle \boldsymbol{N}^{\mathrm{f}}_{ij}(t)\boldsymbol{N}^{\mathrm{f}}_{kl}(t')\rangle = k_{\mathrm{B}}T\,\boldsymbol{1}\,(\delta_{ik}\delta_{jl} + \delta_{il}\delta_{jk})\,\delta(t-t').$$

Then we can rewrite our random force and torque terms in the form of Eqs. (24) and (25).

Simulation parameters and units

In the subsections "Thermodynamic consistency" and "Pressure driven flows" of "Application examples", the natural time unit t_0 is given by the inertial time unit $t_0 = \sqrt{m\sigma^2/k_{\mathrm{B}}T}$ and we choose $\gamma_{\mathrm{R}} = \pi k_{\mathrm{B}}Tt_0$, $\gamma = \frac{3}{4R^2}\gamma_{\mathrm{R}} = 3\pi k_{\mathrm{B}}Tt_0/\sigma^2$, corresponding to the friction parameters of a spherical particle in a Newtonian fluid with viscosity $\eta = 1\,k_{\mathrm{B}}Tt_0/\sigma$ (i.e., $\gamma_{\mathrm{R}} = 8\pi\eta R^3$, $\gamma = 6\pi\eta R$). Furthermore, the parameter ϵ in the WCA potential (Eq. (34)) is set to $\epsilon = k_{\mathrm{B}}T$. The results presented in these subsections were acquired using HOOMD-blue[56].

In the subsection "Active particles and motility-induced phase separation", the results are given in terms of the diffusive time unit $t_{\mathrm{R}} = \gamma_{\mathrm{R}}/k_{\mathrm{B}}T$. Here, we choose the parameters to be the same as in a previous MIPS study without frictional contacts[51], i.e., $\gamma = \gamma_{\mathrm{R}}/\sigma^2 = t_{\mathrm{R}}k_{\mathrm{B}}T/\sigma^2$ and $m = 0.05\,k_{\mathrm{B}}T\,(t_{\mathrm{R}}/\sigma)^2$, and $\epsilon = 10k_{\mathrm{B}}T$. The results were obtained with LAMMPS[57].

Data availability

The data that support the findings of this study are available from the corresponding author upon request. The numerical source data for the graphs and the scripts used to generate data (in LAMMPS and HOOMD-blue) are available at https://doi.org/10.48328/tudatalib-1838(version 3).

Code availability

The LAMMPS simulation code is available at https://doi.org/10.48328/tudatalib-1838. The HOOMD simulation code has been merged with HOOMD-blue and is available in the version 6.1.0, see https://hoomd-blue.readthedocs.io/en/v6.1.0/hoomd/md/pair/module-friction.html for a documentation.

Received: 10 July 2025; Accepted: 30 March 2026;
Published online: 21 April 2026

References

1. Bowden, F. P., Tabor, D. Friction: An Introduction to Tribology. Anchor Press: Garden City, New York, 1973.
2. Popova, E. & Popov, V. L. The research works of coulomb and amontons and generalized laws of friction. *Friction* **3**, 183–190 (2015).
3. Cundall, P. A. & Strack, O. D. L. A discrete numerical model for granular assemblies. *Geotechnique* **29**, 47–65 (1979).
4. Elperin, T. & Golshtein, E. Comparison of different models for tangential forces using the particle dynamics method. *Phys. A* **242**, 332 (1997).
5. Herrmann, H. J. & Luding, S. Modeling granular media on the computer. *Contin. Mech. Thermodyn.* **10**, 189–231 (1998).
6. Luding, S. Anisotropy in cohesive, frictional granular media. *J. Phys. Condens. Matter* **17**, S2623 (2005).
7. Silbert, L. E. et al. Granular flow down an inclined plane: Bagnold scaling and rheology. *Phys. Rev. E* **64**, 051302 (2001).
8. Silbert, L. E. Jamming of frictional spheres and random loose packing. *Soft Matter* **6**, 2918–2924 (2010).
9. Gennes, P.-G. d Brownian motion with dry friction. *J. Stat. Phys.* **119**, 953–962 (2005).
10. Touchette, H., Van der Straeten, E. & Just, W. Brownian motion with dry friction: Fokker–planck approach. *J. Phys. A: Math. Theor.* **43**, 445002 (2010).

11. Baule, A. & Sollich, P. Singular features in noise-induced transport with dry friction. *Europhys. Lett.* **97**, 20001 (2012).
12. Agarwal, G. S. Fluctuation-dissipation theorems for systems in non-thermal equilibrium and applications. *Z. f.ür. Phys.* **252**, 25–38 (1972).
13. Semeraro, M., Gonnella, G., Lippiello, E. & Sarracino, A. Diffusion properties of a Brownian ratchet with Coulomb friction. *Symmetry* **15**, 200 (2023).
14. Antonov, A. P., Caprini, L., Scholz, C. & Löwen, H. Inertial active matter with coulomb friction. *Phys. Rev. Lett.* **133**, 198301 (2024).
15. Wagner, N. J. & Brady, J. F. Shear thickening in colloidal dispersions. *Phys. Today* **62**, 27–32 (2009).
16. Seto, R., Mari, R., Morris, J. F. & Denn, M. M. Discontinuous shear thickening of frictional hard-sphere suspensions. *Phys. Rev. Lett.* **111**, 218301 (2013).
17. Wyart, M. & Cates, M. E. Discontinuous shear thickening without inertia in dense non-brownian suspensions. *Phys. Rev. Lett.* **112**, 098302 (2014).
18. van der Meer, B., Yanagishima, T. & Dullens, R. P. A. Attraction-enhanced emergence of friction in colloidal matter. *Phys. Rev. Lett.* **134**, 078202 (2025).
19. Guy, B. M., Hermes, M. & Poon, W. C. Towards a unified description of the rheology of hard-particle suspensions. *Phys. Rev. Lett.* **115**, 088304 (2015).
20. Lin, N. Y. et al. Hydrodynamic and contact contributions to continuous shear thickening in colloidal suspensions. *Phys. Rev. Lett.* **115**, 228304 (2015).
21. Royer, J. R., Blair, D. L. & Hudson, S. D. Rheological signature of frictional interactions in shear thickening suspensions. *Phys. Rev. Lett.* **116**, 188301 (2016).
22. Comtet, J. et al. Pairwise frictional profile between particles determines discontinuous shear thickening transition in non-colloidal suspensions. *Nat. Commun.* **8**, 15633 (2017).
23. Hsu, C.-P., Ramakrishna, S. N., Zanini, M., Spencer, N. D. & Isa, L. Roughness-dependent tribology effects on discontinuous shear thickening. *Proc. Natl. Acad. Sci. USA* **115**, 5117–5122 (2018).
24. Morris, J. F. Shear thickening of concentrated suspensions: Recent developments and relation to other phenomena. *Annu. Rev. Fluid Mech.* **52**, 121–144 (2020).
25. Nie, P. et al. Frictional active Brownian particles. *Phys. Rev. E* **102**, 032612 (2020).
26. Abaurrea-Velasco, C., Lozano, C., Bechinger, C. & de Graaf, J. Autonomously probing viscoelasticity in disordered suspensions. *Phys. Rev. Lett.* **125**, 258002 (2020).
27. Narinder, N., Bos, M. F., Abaurrea-Velasco, C., de Graaf, J. & Bechinger, C. Understanding enhanced rotational dynamics of active probes in rod suspensions. *Soft Matter* **18**, 6246–6253 (2022).
28. Nguyen, N. H., Klotsa, D., Engel, M. & Glotzer, S. C. Emergent collective phenomena in a mixture of hard shapes through active rotation. *Phys. Rev. Lett.* **112**, 075701 (2014).
29. Soni, V. et al. The odd free surface flows of a colloidal chiral fluid. *Nat. Phys.* **15**, 1188–1194 (2019).
30. Tan, T. H. et al. Odd dynamics of living chiral crystals. *Nature* **607**, 287–293 (2022).
31. Zhao, Z., Yang, M., Komura, S. & Seto, R. Odd viscosity in chiral passive suspensions. *Front. Phys.* **10**, 951465 (2022).
32. Huang, R., Mandal, R., Scheibner, C. & Vitelli, V. Odd elasticity in driven granular matter. preprint https://arxiv.org/abs/2311.18720 (2023).
33. Fruchart, M., Scheibner, C. & Vitelli, V. Odd viscosity and odd elasticity. *Annu. Rev. Condens. Matter Phys.* **14**, 471–510 (2023).
34. Risken, H. *The Fokker-Planck Equation*. Springer Series in Synergetics 2nd edn (Springer Berlin, Heidelberg, 1996).
35. Paul, W. & Baschnagel, J. *Stochastic Processes* 2nd edn (Springer Berlin, Heidelberg, 2013).
36. Hänggi, P. & Thomas, H. Stochastic processes – time evolution, symmetries and linear response. *Phys. Rep.* **88**, 207–319 (1982).
37. Klimontovich, Y. L. Itô, stratonovich and kinetic forms of stochastic equations. *Phys. A* **163**, 515–532 (1990).
38. Escudero, C. & Rojas, H. Itô versus Hänggi-Klimontovich. *Physica Scripta* **100**, 125241 (2023).
39. Español, P. & Warren, P. Statistical mechanics of dissipative particle dynamics. *Europhys. Lett.* **30**, 191–196 (1995).
40. Junghans, C., Praprotnik, M. & Kremer, K. Transport properties controlled by a thermostat: an extended dissipative particle dynamics thermostat. *Soft Matter* **4**, 156–161 (2008).
41. Espanol, P. Fluid particle model. *Phys. Rev. E* **57**, 2930–2948 (1998).
42. Weeks, J. D., Chandler, D. & Andersen, H. C. Role of repulsive forces in determining the equilibrium structure of simple liquids. *J. Chem. Phys.* **54**, 5237–5247 (1971).
43. Brady, J. F. & Bossis, G. Stokesian dynamics. *Ann. Rev. Fluid Mech.* **20**, 111–117 (1988).
44. Keaveny, E. E., Pivkin, I. V., Maxey, M. & Karniadakis, G. E. A comparative study between dissipative particle dynamics and molecular dynamics for simple- and complex-geometry flows. *J. Chem. Phys.* **123**, 104107 (2005).
45. Smiatek, J., Allen, M. P. & Schmid, F. Tunable-slip boundaries for coarse-grained simulations of fluid flow. *Eur. Phys. J. E* **26**, 115 (2008).
46. Zhou, J., Belyaev, A., Schmid, F. & Vinogradova, O. Anisotropic flow in striped superhydrophobic channels. *J. Chem. Phys.* **136**, 194706 (2012).
47. Backer, J. A., Lowe, C. P., Hoefsloot, H. C. J. & Iedema, P. D. Poiseuille flow to measure viscosity of particle model fluids. *J. Chem. Phys.* **122**, 154503 (2005).
48. Fedosov, D. A., Karniadakis, G. E. & Caswell, B. Steady shear rheometry of dissipative particle dynamics models of polymer fluids in reverse Poiseuille flows. *J. Chem. Phys.* **132**, 144103 (2010).
49. Cates, M. E. & Tailleur, J. Motility-induced phase separation. *Annu. Rev. Condens. Matter Phys.* **6**, 219–244 (2015).
50. Löwen, H. Inertial effects of self-propelled particles: From active Brownian to active Langevin motion. *J. Chem. Phys.* **152**, 040901 (2020).
51. Hecht, L., Mandal, S., Löwen, H. & Liebchen, B. Active refrigerators powered by inertia. *Phys. Rev. Lett.* **129**, 178001 (2022).
52. Hecht, L. et al. Amep: The active matter evaluation package for Python. *Comput. Phys. Commun.* **309**, 109483 (2025).
53. Bialké, J., Siebert, J. T., Löwen, H. & Speck, T. Negative interfacial tension in phase-separated active brownian particles. *Phys. Rev. Lett.* **115**, 098301 (2015).
54. Levis, D., Codina, J. & Pagonabarraga, I. Active Brownian equation of state: metastability and phase coexistence. *Soft Matter* **13**, 8113–8119 (2017).
55. Sokolov, I. M. Itô, Stratonovich, Hänggi and all the rest: the thermodynamics of interpretation. *Chem. Phys.* **375**, 359–363 (2010).
56. Anderson, J. A., Glaser, J. & Glotzer, S. C. Hoomd-blue: A python package for high-performance molecular dynamics and hard particle Monte Carlo simulations. *Comput. Mater. Sci.* **173**, 109363 (2020).
57. Thompson, A. P. et al. Lammps - a flexible simulation tool for particle-based materials modeling at the atomic, meso, and continuum scales. *Comp. Phys. Comm.* **271**, 108171 (2022).

Acknowledgements

We thank the anonymous reviewers for their careful assessment of the manuscript and numerous helpful comments. FS thanks Ralf Metzler for pointing out the Hänggi-Klimontovich formalism. This work was funded by the Deutsche Forschungsgemeinschaft (DFG) via Grant 233630050, TRR 146, Project A3, and A9. The authors gratefully acknowledge the computing time provided to them on the high-performance computer Mogon2 and Mogon NHR South-West.

Author contributions

F.S. and B.L. designed the research and supervised the work. F.S. developed the theory with support from K.H. and K.D.; K.H. and K.D. implemented the simulation codes (HOOMD-blue and LAMMPS, respectively), performed the simulations, analyzed and visualized the data. All authors contributed to the writing of the original draft, K.H. and F.S. finalized the manuscript, and all authors reviewed it.

Funding

Open Access funding enabled and organized by Projekt DEAL.

Competing interests

The authors declare no competing interests.

Additional information

Supplementary information The online version contains supplementary material available at https://doi.org/10.1038/s42005-026-02624-5.

Correspondence and requests for materials should be addressed to Friederike Schmid.

Peer review information *Communications Physics* thanks the anonymous reviewers for their contribution to the peer review of this work. A peer review file is available.